Supporting Information:
Plasma Catalysis for CO_2 Hydrogenation: Unlocking New Pathways Towards CH_3OH

Roel Michiels, Yannick Engelmann and Annemie Bogaerts*
Research group PLASMANT, University of Antwerp, Department of Chemistry
Universiteitsplein 1, BE-2610 Wilrijk-Antwerp, Belgium

*: annemie.bogaerts@uantwerpen.be

S.1 Thermal catalysis: TOF of the main products and surface coverages – Comparison of Model 1 and 2

Our first model for thermal catalysis predicted that the most important CO_2 hydrogenation products are, in decreasing order of importance, HCOOH, H_2O and H_2CO and CH_3OH (see Figure S.1 (a)). However, experimentally CH_3OH is the expected product for CO_2 hydrogenation on a Cu catalyst, and HCOOH and H_2CO formation are not experimentally observed.[1,2] Furthermore, experimental studies found the surface to be covered with HCOO*,[3] while our first model predicted H* and CO* to be the main surface species (see Figure S.1 (b)). Based on these arguments and to better agree with experiments on the industrially used Cu/ZnO catalyst, we decided to turn off desorption of HCOOH and H_2CO in our model.

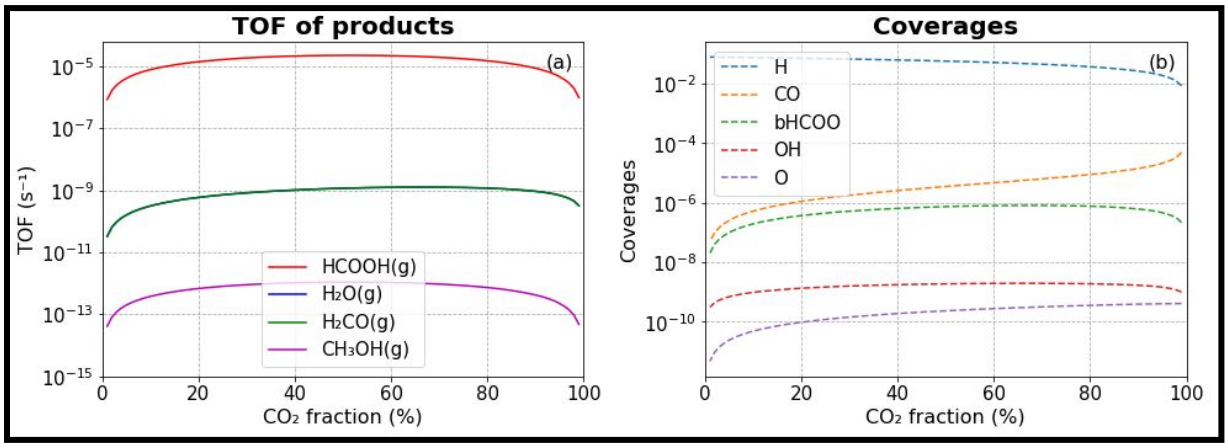

Figure S.1: TOF of products (a) and coverages of the five most abundant surface species (b) as a function of the CO_2 fraction in the H_2/CO_2 gas mixture (T_g = 400 K, p_{tot} = 1 bar), for Model 1. The TOF of H_2CO and H_2O are equal, hence their lines on the plot overlap.

In addition, as will be discussed further on, the rate-limiting step for CH_3OH formation via the formate pathway was found to be H_2COOH* dissociation. This is due to the reaction set of Zhao et al.,[4] who reported a barrier of 1.36 eV. As Zhao et al., are the only authors to report this step as being rate-limiting, the enthalpic barrier for H_2COOH* dissociation was lowered to 0.74 eV in our model, i.e., the value reported by Grabow et al.[5]

The calculation results after implementing these changes are displayed in figure S.2, and agree better with literature. This version of the model is called Model 2, while the original version is Model 1. With these changes, now only CH_3OH and H_2O are produced (figure S.2 (a)). The CH_3OH TOF for Model 2 is equal to the TOF of H_2CO for Model 1, indicating that all H_2CO is now converted to CH_3OH.

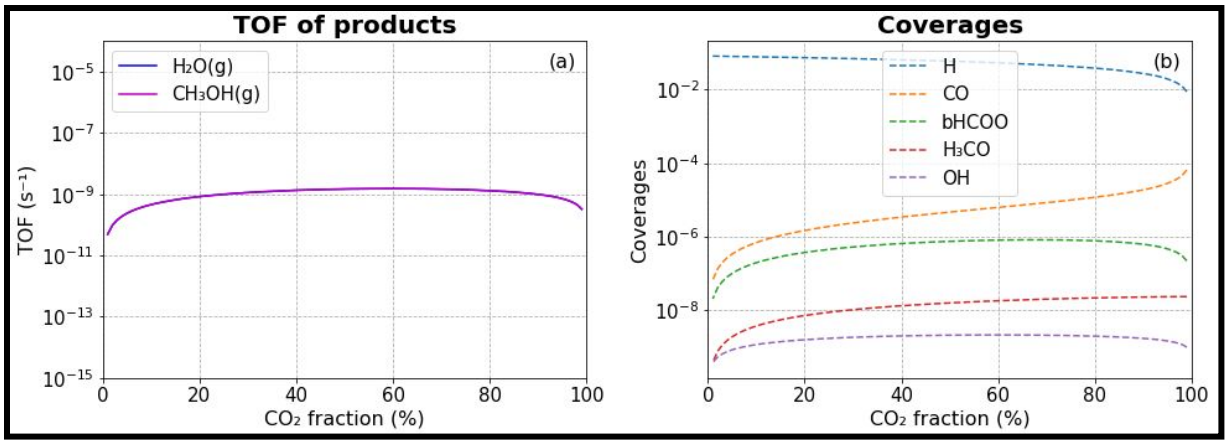

Figure S.2: TOF of products (a) and coverages of the five most abundant surface species (b) as a function of the CO_2 fraction in the H_2/CO_2 gas mixture, when desorption of HCOOH and H_2CO is not allowed (T_g = 400 K, p_{tot} = 1 bar), i.e. Model 2. The TOF of CH_3OH and H_2O are equal, hence the lines on the plot overlap.

The coverages predicted by Model 2, however, do not agree better with literature. Experimental studies found the surface to be covered with HCOO*.[3] The most abundant surface species in Model 2 is still H* with a coverage around 0.05, depending on the H_2 content in the gas phase. CO* and bHCOO* can also be found on the surface, but their coverage is at least three orders of magnitude smaller than the H* coverage. The only difference with Model 1 is the higher coverage of H_3CO*. This is caused by not allowing H_2CO formation. Most of the surface sites are still unoccupied. Hence, our model is not able to predict the experimental coverages, probably due to reaction barriers or energies that are not accurate enough. We chose not to change the energy values in the model as it is not immediately clear which values need to be changed or how they should be changed. More consistent DFT data is needed, so that this can be further improved in the future.

The H_2/CO_2 ratio does not seem to have a big influence in either case. In Model 1 it does not influence the product selectivity and there is only a small impact on the absolute TOFs for both cases. The TOFs only vary within three orders of magnitude. When the CO_2 content is high, i.e. >80%, the TOF of CH_3OH decreases with one order of magnitude compared to a 1:1 mixture. When the H_2 content is high, i.e. >80%, the TOF of CH_3OH decreases up to two orders of magnitude compared to a 1:1 mixture. Similarly, the coverages do not drastically change when varying the CO_2 content. The values can vary over several orders of magnitude, but the order of the coverages stays the same.

It should be noted that thermal catalytic hydrogenation of CO_2 is not completely selective towards CH_3OH, but also produces CO. CO is not reported as a product, since we did not allow for CO* desorption in the model when the initial pressure of CO is equal to zero, as is the case in thermal catalysis. When CO desorption is allowed, and follows the PED from Zhao et al.[4], CO_2 is converted with near 100 % selectivity to CO. This should lead to a fast increase in CO pressure, which then promotes CO adsorption after which the CH_3OH selectivity would start increasing. However, this cannot be accounted for by the model, as the gas phase pressures are fixed, and the instantaneous TOFs at 0% conversion, would poorly represent realistic TOFs. In the future, this problem can be fixed by extending the model to also solve for the gas phase partial pressures.

Importantly, this assumption was not necessary in the plasma catalysis model (see further) as CO was part of the plasma phase composition (and the reverse reaction of CO adsorption was not zero). For this reason, the aforementioned assumption does not change the new potential pathways in plasma catalysis, which is the main research goal of the paper.

As far as the main CH_3OH formation pathways are concerned, Model 2 predicts that the HCO* hydrogenation is responsible for ca. 75% of H_2CO* formation, while according to Model 1, the rate of this process is 10 orders of magnitude higher than the rate of H_2COOH* dissociation into H_2CO* and OH*. This difference is due to HCOOH* desorption in Model 1, i.e. hydrogenation of HCOO* leads to

formation of HCOOH* and subsequent desorption of HCOOH, rather than to CH_3OH formation. Hydrogenation of HCOO* to H_2COO* also leads to HCOOH formation, as H_2COOH* reacts to HCOOH*. In Model 2, on the other hand, HCOO* hydrogenation leads to CH_3OH formation through a HCOOH* or H_2COO* intermediate, since desorption of HCOOH* is no longer allowed. At a 1:1 H_2/CO_2 ratio, the path through H_2COO* is responsible for ca. 17% of H_2COOH* formation. Since the main formation mechanism of CH_3OH is the same for both Model 1 and 2, the higher CH_3OH TOF and higher H_3CO* coverage in Model 2 are caused by disallowing the desorption of H_2CO*.

S.2 Plasma catalysis: Effect of radicals and intermediates – TOF of the main products and surface coverages

We present here the TOFs of the main products and the surface coverages when gradually adding the plasma-generated radicals and intermediates to the model.

(a) Effect of CO, O, H, OH and H_2O

The results when adding CO, O, H, OH and H_2O to the gas phase are displayed in figure S.3. It is clear that adding these species has a large impact on the product TOFs (cf. Figure S.3 vs. Figure S.2). H_2 is no longer consumed but formed at the surface, the H_2O TOF is no longer equal to the TOF of CH_3OH, and most importantly, the CH_3OH TOF has increased with six-seven orders of magnitude compared to thermal catalysis. The TOFs of H_2 and H_2O are independent from the H_2/CO_2 ratio.

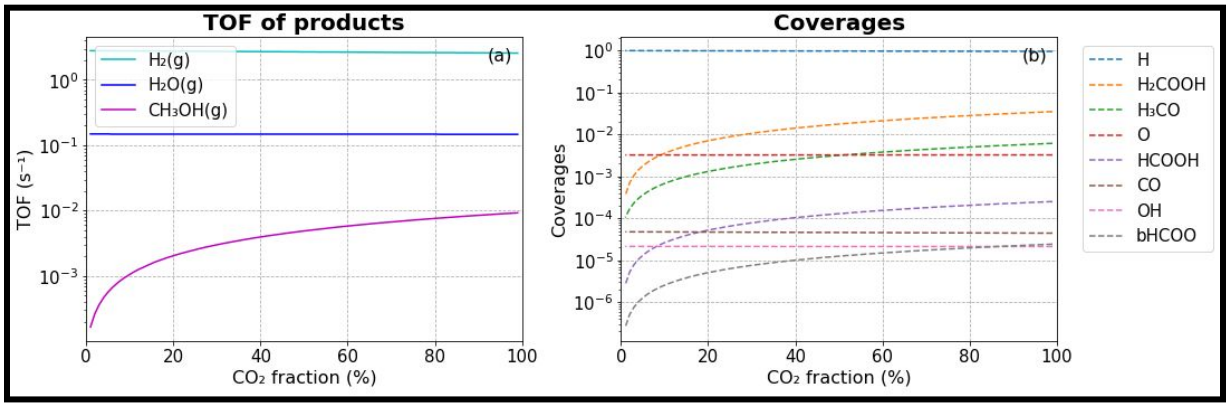

Figure S.3: TOF of products (a) and coverages of the eight most abundant surface species (b) as a function of the CO_2 fraction in the H_2/CO_2 gas mixture, when CO, O, H, OH and H_2O are added to the gas phase, with the pressures defined by table 2 in the main paper.

H* is still the most abundant adsorbate, and its coverage has increased with almost two orders of magnitude and varies around 0.97, depending on the CO_2 content (Figure S.3 (b)). Except for CO* and bHCOO*, the coverage of the most abundant adsorbates has increased by several orders of magnitude. The H_2COOH* and HCOOH* coverages have increased the most: in thermal catalysis their coverage is at most equal to 10^{-14} and 10^{-10}, respectively, while it is now equal to 10^{-2} and 10^{-4}. The plasma thus creates more hydrogenated species on the surface than in thermal catalysis. The CO*, O* and H* coverages seem to be independent of the CO_2 content in the gas mixture, because the radical pressures are kept constant, and thus independent of the CO_2 pressure. This would be a useful improvement for future models.

(b) Effect of H_2CO and HCO

Figure S.4 illustrates the TOFs of the main products, as a function of the H_2CO and HCO pressure in the gas phase. Adding these species to the gas phase did not impact the overall TOFs of the products or the surface coverages. This can be explained by the lower partial pressures of H_2CO and HCO in the plasma, i.e., 10^{-6} and 10^{-11} bar, respectively (Table 2 in the main paper), which leads to adsorption rates that are smaller than the production rates of HCO* and H_2CO* at the surface. For H_2CO, this might

seem surprising as its pressure is equal to the partial pressure of H and higher than the partial pressure of O and OH. However, due to the presence of CO in the gas phase, the H_2CO* TOF is already 10^{-3} s^{-1} while the adsorption rate of H_2CO is only $4.32x10^{-8}$ s^{-1}, i.e. too small to make a difference.

As depicted in Figure S.4, the pressure of H_2CO would have to increase by at least three orders of magnitude (compared to the value listed in table 2 in the main paper) to affect the CH_3OH production. Since H_2CO is not produced by the catalyst, such higher pressures are considered unlikely. Likewise, the HCO pressure would have to increase at least four orders of magnitude to affect the catalyst chemistry.

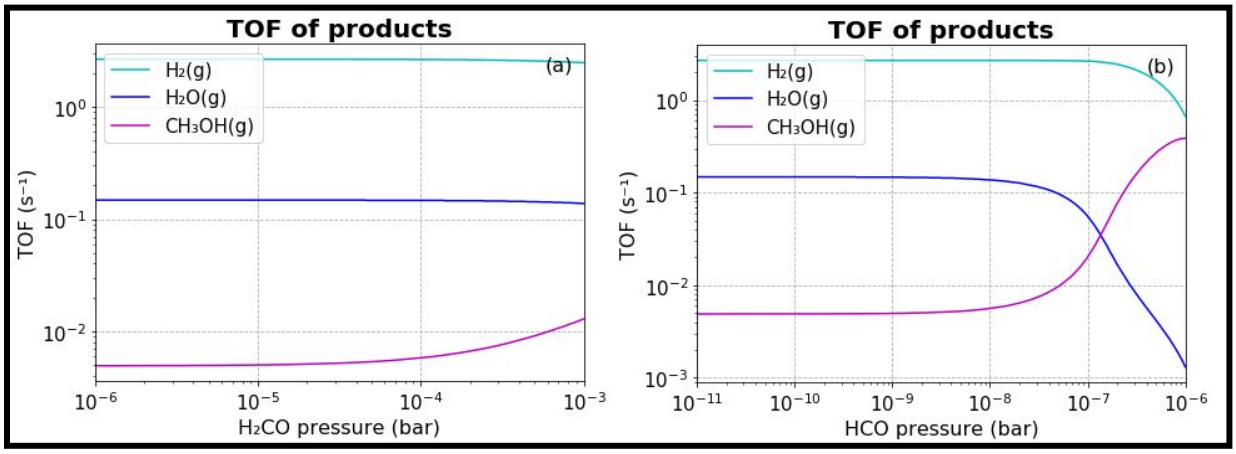

Figure S.4: TOFs of the products as a function of H_2CO pressure (a) and HCO pressure (b).

Despite the fact that H_2CO and HCO do not impact the CH_3OH (and other products) TOFs, we briefly discuss their reactions, as they might still result in CH_3OH formation, if they would have higher pressures in the plasma. As discussed above, HCO* mainly reacts with O* and H* to form bHCOO* and H_2CO*, respectively.

The reason for the low H_2CO adsorption rate is depicted in Figure S.5. It shows that, under plasma conditions, H_2CO from the gas phase is mainly consumed by Eley-Rideal (ER) reactions with O* and H*, resulting in H_2COO* and H_2COH* formation, respectively. This result shows that ER reactions can be important under plasma conditions, because of the high surface coverage of radicals. The reaction with O* is faster, despite the higher H* coverage, since the ER reaction with O* only has a barrier of 0.07 eV, while the reaction with H* has a barrier of 0.70 eV. Of course, these energy values should be treated with care, as they were only reported once (by Zhao et al.[4]) The formed H_2COO* will further react to CH_3OH via the formate pathway, and thus the ER reaction with O* essentially skips the HCOO* and HCOOH* hydrogenation steps, which are rate-limiting. The ER reaction with H* generates H_2COH*, which will be hydrogenated and thus converted into CH_3OH in only one step. Hence, these pathways would be very favourable for CH_3OH formation, but unfortunately the H_2CO pressure is too low for the reactions to reach a high enough rate.

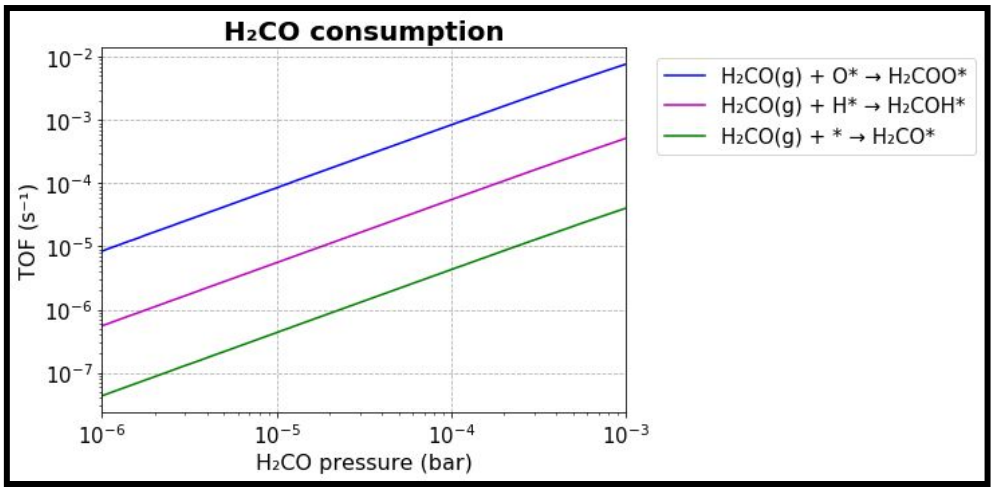

Figure S.5: TOFs the H_2CO consumption reactions as a function of H_2CO pressure.

(c) Effect of CH_2, CH_3 and CH_4

Finally, the product TOFs upon adding CH_2, CH_3 and CH_4 to the gas phase are displayed in Figure S.6. Unsurprisingly, CH_4 is produced at the surface, but only at very low TOF. It has to be noted that reactions of the type CH_x* + O(H)* were not included in the model. These reactions can possibly be advantageous for CH_3OH formation. However, they typically have a higher barrier than hydrogenation reactions. For instance, the activation energy of CH_2* + O* on Cu is 1.53 eV, thus almost 1 eV higher than the activation energy of hydrogenation (0.61 eV).[6] Furthermore, the H* coverage is higher than the O* coverage and the CH_2 and CH_3 pressure in the plasma will probably be too low for these kind of reactions to make a significant contribution to CH_3OH formation.

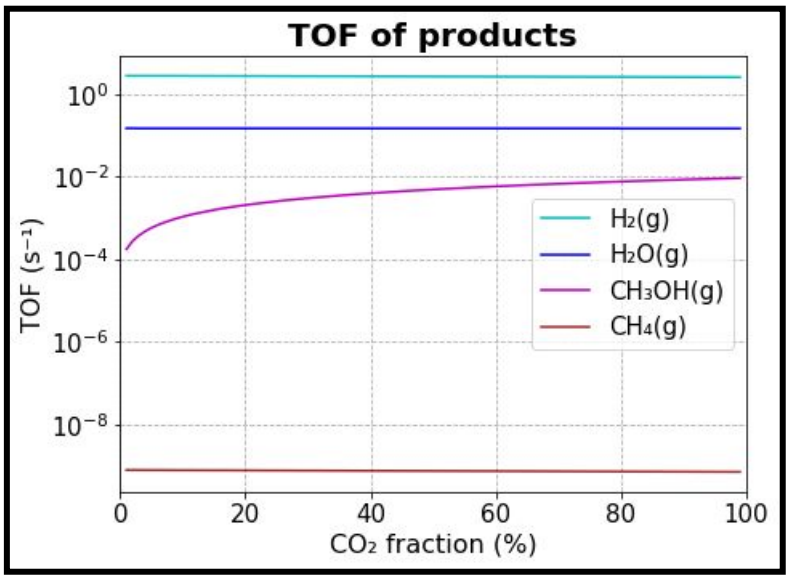

Figure S.6: TOFs as a function of the CO_2 fraction in the H_2/CO_2 gas mixture, when CH_2, CH_3 and CH_4 are added to the gas phase, with the pressures defined by table 2 in the main paper.

S.3 Impact of using the experimental adsorption energy of CO on the results

In this section, we discuss the impact of using the experimental value of -0.52 eV[7] for the adsorption energy of CO, instead of the DFT value of -1.06 eV. As CO desorption is not allowed in thermal catalysis for reasons already discussed in section 3.5 of the main paper, changing the adsorption energy will

only have an effect on the results for plasma catalysis, specifically the impact of CO generated by the plasma. We will focus on the differences in the results when CO, O, H, OH and H_2O are added to the gas phase, i.e. we will compare with the results discussed in section S.2(a). The results, when the CO adsorption energy is changed, are displayed in Figure S.7. When we compare this figure to figure S.3, the TOF of CH_3OH remains unchanged. This is to be expected as the main reaction pathway for CH_3OH synthesis in plasma catalysis is the formate pathway, initiated by $CO_2 + H^* \rightarrow HCOO^*$ (reaction R5 in Table 1) and is not altered by a change in the CO adsorption energy. The major difference is the decreased coverage of CO*, which is no longer visible on the figure, as it is now only 4.6×10^{-12}, seven orders of magnitude lower compared to the coverage in Figure S.3.

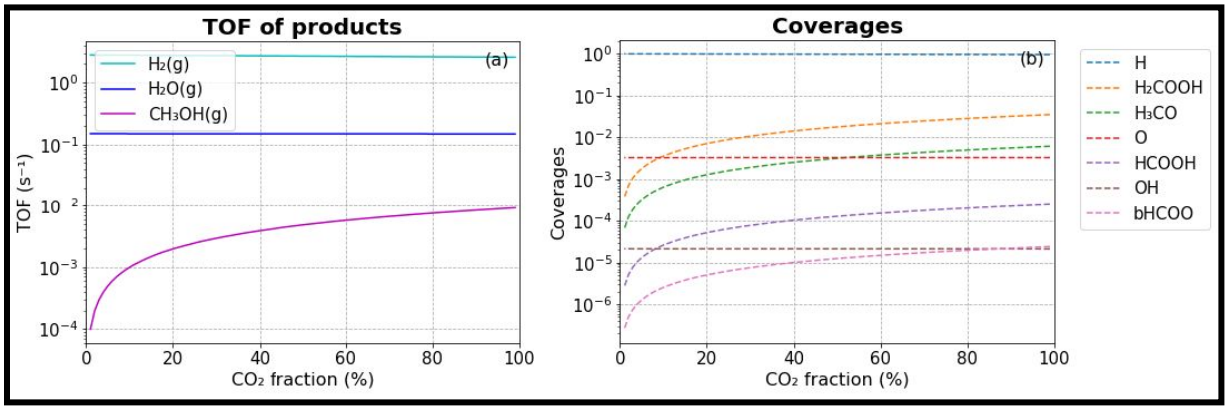

Figure S.7: TOF of products (a) and coverages of the seven most abundant surface species (b) as a function of the CO_2 fraction in the H_2/CO_2 gas mixture, when CO, O, H, OH and H_2O are added to the gas phase, with the pressures defined by table 2 in the main paper. The CO adsorption energy in the model is now -0.52 eV.

The decreased CO* coverage is due to faster desorption, caused by the lower adsorption energy. Under these assumptions, there is no net CO adsorption from the plasma phase, but a net desorption, promoting the RWGS reaction.

Indeed, because CO desorbs more rapidly, this also means that less CO can contribute to CH_3OH formation via the red and green mechanisms in Figure 6 in the main paper, explaining why the CH_3OH TOF is now 4.88×10^{-3}, which is slightly lower than 4.94×10^{-3}. Hence, the effect on the CH_3OH TOF is very limited. The WGS (yellow path in Figure 6) now occurs in the reverse direction, i.e. CO_2 is partially converted into CO via the RWGS reaction.

These results illustrate the importance of reliable and good DFT data, as the outcome of the model in general heavily depends on the input data. This DFT data is much needed for further optimization of the models specifically, and the plasma-catalytic processes in general. To fully understand the influence of CO produced by the plasma on the mechanisms, a combined plasma-surface chemistry model that simultaneously calculates gas phase and surface reactions, by introducing additional rate equations for the gas phase species, should be developed. Such a model is beyond the scope of this paper, but can be developed based on the presented model and results.

S.4 Plasma Catalysis: Effects of vibrational excitation

(a) Effect of CO_2 asymmetric stretching mode excitation on CO_2 dissociative adsorption

The effect of excitation of the asymmetric stretching vibration of CO_2 on the rate coefficient of dissociative adsorption is depicted in figure S.8. There are two full lines depicted in the figure. The first one is for $\alpha = 0.45$, which is the value calculated from the Fridman-Macheret formula when using the original value of the reaction enthalpy from literature. When we modify the value of the reaction enthalpy to make all the pathways in the model thermodynamically consistent, then $\alpha = 0.56$. We calculated α for both reaction enthalpies, as their difference is relatively large (0.87 eV).

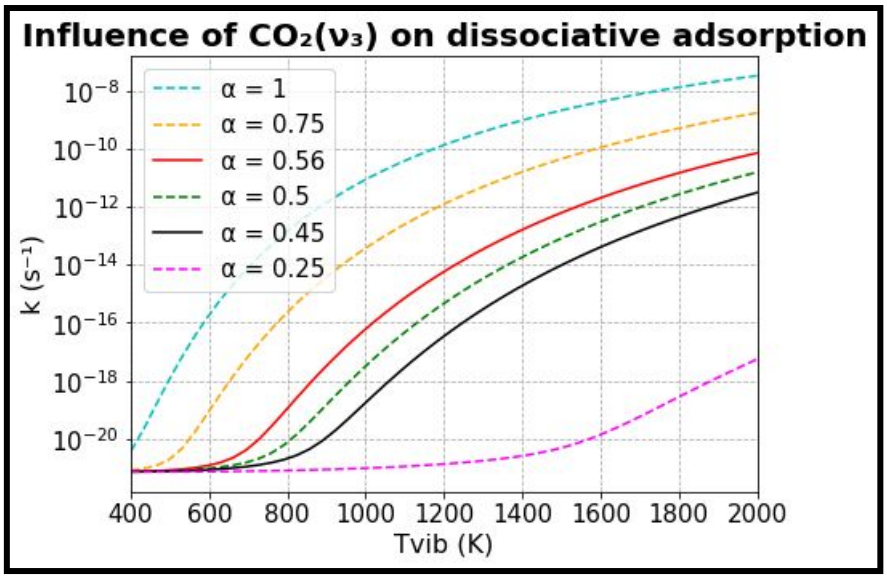

Figure S.8: Influence of the excitation of the asymmetric stretching mode of CO_2 on the rate coefficient of dissociative adsorption as a function of the vibrational temperature, with T_g = 400K. The full lines indicate the values when α is calculated from the Fridman-Macheret formula.

It is clear that excitation of this asymmetric stretching mode increases the rate coefficient of dissociative CO_2 adsorption, but even when T_{vib} = 2000 K and the Fridman-Macheret parameter α = 1 (see meaning in section 3.4 of the main paper), this rise is not large enough for the reaction to actually affect the surface chemistry. It is also clear that the impact of vibrational excitation is heavily dependent on the α parameter: the higher its value, the bigger the impact on the rate coefficient.

Furthermore, as the vibrational temperature of the asymmetric stretching mode of CO_2 in a DBD plasma is typically below 1000 K,[8] the rate coefficient for dissociative adsorption will only rise with two orders of magnitude (for α = 0.56). This is not large enough to make the reaction rate of any significance. Indeed, the reaction rate of dissociative adsorption of CO_2 in thermal catalysis is several orders of magnitude lower than the reaction rate for CO_2 loss through HCOO* or COOH* formation.

(b) Effect of excitation of the asymmetric stretching and bending mode on the formation of HCOO* and COOH*

Figure S.9 depicts the impact of excitation of the asymmetric stretching mode (a) and bending mode (b) on the rate coefficient of HCOO* formation. The influence of both modes is similar, despite the fact that the asymmetric stretching mode levels have a higher energy, i.e. $\tilde{\nu}_2$ = 672.85 cm^{-1} and $\tilde{\nu}_3$ = 2393.32 cm^{-1}.[8] This similar influence can be explained by the balance between the energy of the levels and their occupation. The excited levels of the bending mode will be more occupied than the excited levels of the asymmetric stretching mode, because the latter have a higher energy. This leads the bending mode excitation to cause a larger increase of the rate coefficient than excitation of the asymmetric stretch at lower vibrational temperatures, while at higher vibrational temperatures the effect is similar. At typical plasma conditions, the vibrational temperature of the bending mode of CO_2 is lower than the vibrational temperature of the asymmetric stretching mode.[9,10] This implies that excitation of the asymmetric stretch might have a bigger impact. However, Quan et al.[11], reported that the decrease of the OCO angle is almost entirely responsible for the barrier of HCOO* formation, thus it is reasonable to assume that the bending mode will be more efficient in supplying energy to reach the transition state, i.e. will have a higher α than the asymmetric stretching mode. This illustrates one of the shortcomings of the Fridman-Macheret formula, namely it assumes the same value of α for different modes. Hence, we expect bending mode excitation to be equally or more important than excitation of the asymmetric stretching mode for HCOO* formation, depending on the vibrational temperatures of both normal modes.

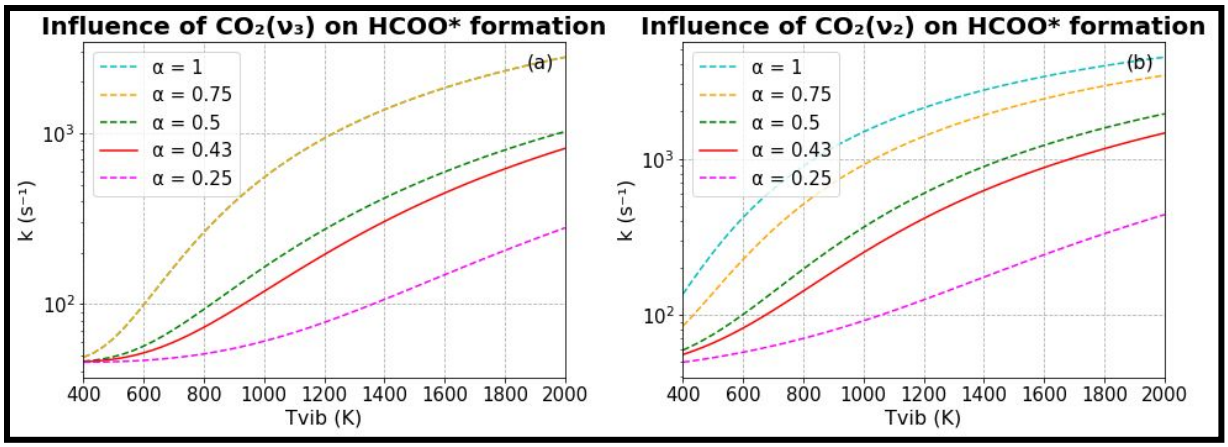

Figure S.9: Effect of the excitation of the asymmetric stretching mode of CO_2 (a) and excitation of the bending mode of CO_2 (b) on the rate coefficient of HCOO* formation through an ER mechanism, as a function of the vibrational temperature, with T_g = 400K. The full lines indicate the values when α is calculated from the Fridman-Macheret formula.

The maximum increase of the rate coefficient of HCOO* formation is only 1-2 orders of magnitude over the entire range of vibrational temperatures (see Figure S.9), depending on the value of α. This is limited compared to the rise of the rate coefficient of dissociative adsorption of CO_2 (see Figure S.8). This can be explained by the fact that dissociative adsorption of CO_2 has a higher barrier than the ER reaction towards HCOO*, and vibrational excitation thus has more potential to lower said barrier.

Similarly, the effect of vibrational excitation on the ER reaction towards COOH*, is larger than the effect on the ER reaction towards HCOO*, because the former reaction has a higher barrier. However, HCOO* formation remains kinetically favoured over COOH* formation.

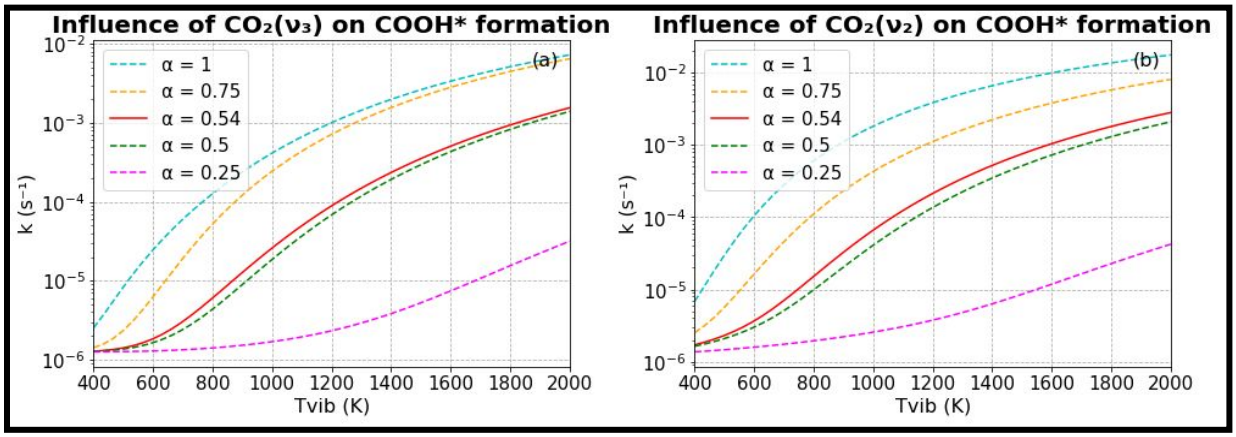

Figure S.10: Effect of the excitation of the asymmetric stretching mode of CO_2 (a) and of the bending mode of CO_2 (b) on the rate coefficient of COOH* formation through an ER mechanism, as a function of the vibrational temperature, with T_g = 400K. The full lines indicate the values when α is calculated from the Fridman-Macheret formula.

References

(1) Porosoff, M. D.; Yan, B.; Chen, J. G. Catalytic Reduction of CO2 by H2 for Synthesis of CO, Methanol and Hydrocarbons: Challenges and Opportunities. *Energy Environ. Sci.* **2016**, *9*, 62–73.

(2) Álvarez, A.; Bansode, A.; Urakawa, A.; Bavykina, A. V.; Wezendonk, T. A.; Makkee, M.; Gascon, J.; Kapteijn, F. Challenges in the Greener Production of Formates/Formic Acid, Methanol, and

DME by Heterogeneously Catalyzed CO2 Hydrogenation Processes. *Chem. Rev.* **2017**, *117*, 9804–9838.

(3) Yang, Y.; Mims, C. A.; Disselkamp, R. S.; Kwak, J. H.; Peden, C. H. F.; Campbell, C. T. (Non)Formation of Methanol by Direct Hydrogenation of Formate on Copper Catalysts. *J. Phys. Chem. C* **2010**, *114*, 17205–17211.

(4) Zhao, Y. F.; Yang, Y.; Mims, C.; Peden, C. H. F.; Li, J.; Mei, D. Insight into Methanol Synthesis from CO2 Hydrogenation on Cu(1 1 1): Complex Reaction Network and the Effects of H2O. *J. Catal.* **2011**, *281*, 199–211.

(5) Grabow, L. C.; Mavrikakis, M. Mechanism of Methanol Synthesis on Cu through CO2 and CO Hydrogenation. *ACS Catal.* **2011**, *1*, 365–384.

(6) Zuo, Z. J.; Wang, L.; Han, P. De; Huang, W. Insights into the Reaction Mechanisms of Methanol Decomposition, Methanol Oxidation and Steam Reforming of Methanol on Cu(111): A Density Functional Theory Study. *Int. J. Hydrogen Energy* **2014**, *39*, 1664–1679.

(7) Govind, N.; Wang, Y. A.; Carter, E. A. Electronic-Structure Calculations by First-Principles Density-Based Embedding of Explicitly Correlated Systems. *J. Chem. Phys.* **1999**, *110*, 7677–7688.

(8) Kozák, T.; Bogaerts, A. Splitting of CO2 by Vibrational Excitation in Non-Equilibrium Plasmas: A Reaction Kinetics Model. *Plasma Sources Sci. Technol.* **2014**, *23*, 045004.

(9) Klarenaar, B. L. M.; Engeln, R.; Van Den Bekerom, D. C. M.; Van De Sanden, M. C. M.; Morillo-Candas, A. S.; Guaitella, O. Time Evolution of Vibrational Temperatures in a CO2 Glow Discharge Measured with Infrared Absorption Spectroscopy. *Plasma Sources Sci. Technol.* **2017**, *26*, 115008.

(10) Urbanietz, T.; Böke, M.; Schulz-Von Der Gathen, V.; Von Keudell, A. Non-Equilibrium Excitation of CO2 in an Atmospheric Pressure Helium Plasma Jet. *J. Phys. D. Appl. Phys.* **2018**, *51*, 345202.

(11) Quan, J.; Muttaqien, F.; Kondo, T.; Kozarashi, T.; Mogi, T.; Imabayashi, T.; Hamamoto, Y.; Inagaki, K.; Hamada, I.; Morikawa, Y.; et al. Vibration-Driven Reaction of CO2 on Cu Surfaces via Eley–Rideal-Type Mechanism. *Nat. Chem.* **2019**, *11*, 722–729.